
Learnable In-Context Vector for Visual Question Answering

Yingzhe Peng¹, Chenduo Hao¹, Xu Yang^{1*}, Jiawei Peng¹, Xinting Hu², Xin Geng¹

¹ Key Laboratory of New Generation Artificial Intelligence Technology & Its Interdisciplinary Applications, (Southeast University), Ministry of Education
{yingzhe.peng, 213201447, xuyang_palm, pengjiawei, xgeng}@seu.edu.cn

² Nanyang Technological University
xinting001@e.ntu.edu.sg

Abstract

As language models continue to scale, Large Language Models (LLMs) have exhibited emerging capabilities in In-Context Learning (ICL), enabling them to solve language tasks by prefixing a few in-context demonstrations (ICDs) as context. Inspired by these advancements, researchers have extended these techniques to develop Large Multimodal Models (LMMs) with ICL capabilities. However, applying ICL usually faces two major challenges: 1) using more ICDs will largely increase the inference time and 2) the performance is sensitive to the selection of ICDs. These challenges are further exacerbated in LMMs due to the integration of multiple data types and the combinational complexity of multimodal ICDs. Recently, to address these challenges, some NLP studies introduce non-learnable In-Context Vectors (ICVs) which extract useful task information from ICDs into a single vector and then insert it into the LLM to help solve the corresponding task. However, although useful in simple NLP tasks, these non-learnable methods fail to handle complex multimodal tasks like Visual Question Answering (VQA). In this study, we propose **Learnable ICV** (L-ICV) to distill essential task information from demonstrations, improving ICL performance in LMMs. Experiments show that L-ICV can significantly reduce computational costs while enhancing accuracy in VQA tasks compared to traditional ICL and other non-learnable ICV methods.

1 Introduction

As language models continue to scale up, Large Language Models (LLMs) [1–3] have demonstrated emerging capabilities in In-Context Learning (ICL) [4]: these models can solve language tasks when provided with a few similar examples, termed in-context demonstrations (ICDs), as context. Unlike traditional task-specific fine-tuning, ICL achieves comparable performance without necessitating updates to millions or trillions of model parameters [5]. By prefixing just a handful of data samples to the query input, ICL configures a model’s behavior to produce the corresponding output, thus facilitating rapid adaptation across a wide range of downstream tasks. Inspired by these advancements in the language domain, researchers have extended these techniques to develop Large Multimodal Models (LMMs) with ICL capabilities [6–8].

Employing ICL in LLMs meets two challenges: Firstly, although increasing the number of ICDs typically enhances performance [5], this practice conflicts with computational efficiency constraints. As ICDs are prefixed to the query, the increase in input tokens severely impacts the Transformer’s inference speed, causing a marked slowdown in computational performance. Secondly, the effectiveness of ICL is vulnerable to the selection of demonstrations [4, 9–11], particularly when only

¹Corresponding author.

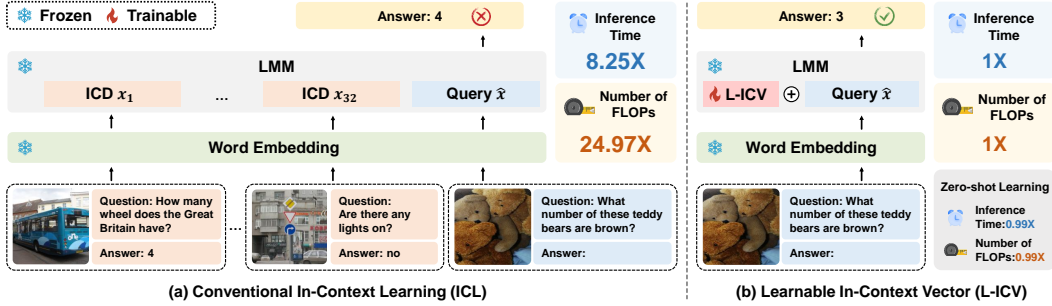


Figure 1: (a) Conventional ICL is more sensitive to the ICD selection and requires more inference time. (b) L-ICV is more robust and reduces inference time by inputting a shift vector.

a limited number are used. It makes the process of choosing demonstrations critical for optimal performance. However, developing selection strategies and measuring the effectiveness of ICDs remain open questions [12–15]. For LMMs, the challenges above are further exacerbated: 1) The computational complexity is significantly increased due to the integration of multiple data types as ICDs (as shown in Figure 1(a)). 2) The task of selecting effective multi-modal ICDs becomes more complex and nuanced, as each modality contributes uniquely to understanding the context [16, 17], further complicating the assessment of their combined effect in demonstration selection.

To alleviate these two challenges, recent research on LLMs has introduced In-Context Vector (ICV) to extract the most useful task information from ICDs, and then use it to directly influence the processing in LLMs [18–20]. For example, [18] proposes that by using multiple demonstrations and a dummy query as inputs, the representation of the last token from a middle layer of the model can be extracted as the vector. This vector is then used to replace the representation of the corresponding token in the same layer during inference, which can achieve performance comparable to ICL. Such in-context vector alleviates the requirement of multiple ICDs during inference, as well as effectively bypasses the complexity of the individual selection of demonstrations by representing the most effective components across many demonstrations.

However, these studies apply non-learnable strategies to extract ICVs, although useful in some simple NLP tasks, lose the efficacy in complex multi-modal tasks like Visual Question Answering (VQA). Our preliminary experiments have demonstrated that directly applying these non-learnable ICVs yields unsatisfactory results. The principal reason is the intrinsic complexity of VQA compared to the language tasks addressed by these non-learnable ICVs. For example, the previous methods focus on simple NLP task, such as Antonym [21] and Country-Capital [19], whose distribution patterns can be easily identified by LLMs. In contrast, as a unified vision-language task, VQA encompasses a diverse array of question types, where each one corresponds to a different vision-understanding task. For instance, questions like “What is this?” or “How many are there?” require classification and counting abilities, respectively. These varied requirements imply that the task information, which non-learnable methods attempt to abstract, cannot be effectively captured by a single ICV.

In this study, to make ICVs abstract more useful VQA task information, we try to distill the task information implied in demonstrations into a single **Learnable ICV (L-ICV)**. Our method is motivated by the observation [18] that ICL can be treated as a process of “shifting” the direction of the latent states of query towards the target, *i.e.*, adding this latent state with a shift vector. Then we hope to learn suitable ICVs to replace the ICDs during inference to shift the direction. To achieve this, we train this L-ICV by minimizing the output distributions of a LMM got by only using this L-ICV and by inputting a few demonstrations. During training, we use different 32-shot randomly sampled demonstrations for different queries to distill task knowledge. Then L-ICV is encouraged to capture the most essential task information from these different combinations by removing the individual characteristics of demonstrations. Moreover, [22] finds that during ICL, different layers of LLM have diverse roles in addressing demonstrations. Then in our method, each layer is assigned with a unique ICV to capture more fine-grained task information.

Our L-ICV inherits the efficiency of previous non-learnable ICVs, *i.e.*, during inference, under the same performance conditions, L-ICV only needs 1/24.97 FLOPs number of 32-shot ICL. Additionally, in VQAV2/OKVQA, L-ICV improves accuracy by 2.36/1.6 compared to 32-shot ICL. We also compare L-ICV to LoRA [23] that when comparable trainable parameters are used, L-ICV requires much fewer training samples than LoRA (500 vs. 8000) to achieve satisfactory performance. Besides,

we design lots of analytical experiments to validate whether L-ICV can better shift the hidden states of queries to the target direction and analyze why previous non-learnable methods fail to solve VQA.

2 Related Work

In-Context Vector: Recently, more and more researchers in NLP have begun to focus on using an In-Context Vector (ICV) to modify the activation values during the forward propagation of LLM to simulate the effect of ICDs in ICL. [18] propose the ‘‘Task Vector’’, which extracts the representation of the middle layer from the LLM during ICL inference as the ICV, and replaces the representation of the same layer during zero-shot inference. Meanwhile, [19] introduced the ‘‘Function Vector’’, which uses attention weight analysis to take the mean of the activation values of the attention heads that most significantly affect the final result in ICL inference as the final ICV. This vector is then directly added to the representation of the middle layer during zero-shot inference to form a new representation. On the other hand, [20] propose ‘‘PCA In-Context Vector’’. They believe that the ICV should be closer to the LLM’s representation of the task output and farther from the task input representation. Thus, they extract the input and output representations of several demonstrations and using PCA to find the overall principal direction as the ICV. These efforts mainly focus on using non-learnable methods to find the specific ICV for NLP tasks, achieving effects similar to ICL in various tasks. However, these methods only are tested on some simple tasks in NLP. When LMMs face with more complex tasks, the performance of these methods remains uncertain.

ICL in LLM: Prompt engineering allows LLMs to tackle specific tasks without requiring fine-tuning [24–26]. A specific form of this approach, ICL, further improves these capabilities by creating prompts that include several demonstrations. ICL has already demonstrated superior performance and good generalization on many tasks [27, 5, 28], and can be easily adapted to downstream tasks. However, the use of ICL faces several issues: first, ICL is very sensitive to the selection and arrangement order of demonstrations [4, 9–11, 29]; poor demonstrations can severely impact ICL performance. Second, too many demonstrations can significantly slow down the inference speed of LLMs [30, 31]. While ICVs can effectively address these two issues, as it can use only queries as input to the model while preserving ICL performance, without the need for demonstrations as input.

ICL in LMM: As the performance of LLMs continues to improve, an increasing number of researchers begin to adapt LLMs to the multimodal domain [32–36]. Relying on the powerful inference capabilities of LLMs, some LMMs have started to exhibit ICL capabilities, such as Flamingo [6] and IDEFICS [7]. Moreover, these models have significantly enhanced their ICL capabilities by concatenating multiple samples as contextual information during the training process. Currently, researchers mainly focus on how to configure demonstrations to address the sensitivity of ICL performance in LMMs. [16, 17] have respectively adopted heuristic retrieval methods for selecting demonstrations in Image Captioning and VQA. However, no researchers have yet extracted ICV from LMMs and evaluated it. Therefore, the effectiveness of ICV in LMMs still needs further exploration. Considering that the IDEFICS model shares the same model structure as Flamingo and possesses stronger ICL capabilities, we primarily focus on valid our method on the IDEFICS model.

3 Learnable In-Context Vector

Here we show how to derive the formulation of the shift vector from Self-Attention (SA) mechanism and then introduce how to design L-ICV based on this formulation. Generally, to implement In-Context Learning (ICL) using a language or multimodal model (LLM/LMM) \mathcal{M} , the input has the following form: $\mathbf{X} = \{\mathbf{X}_D, \hat{\mathbf{x}}\}$, where $\mathbf{X}_D = \{\mathbf{x}_1, \dots, \mathbf{x}_k\}$ represents the concatenation of k In-Context Demonstrations (ICDs), and $\hat{\mathbf{x}}$ denotes the query input, as shown in Figure 2. Given \mathbf{X} as *Key* and *Value*, for each token \hat{x}_i of $\hat{\mathbf{x}}$, applying *Self-Attention (SA)* once yields:

$$\text{SA}(\hat{x}_i, \mathbf{X}, \mathbf{X}) = \text{SA}(\hat{x}_i, \begin{bmatrix} \mathbf{X}_D \\ \hat{\mathbf{x}} \end{bmatrix}, \begin{bmatrix} \mathbf{X}_D \\ \hat{\mathbf{x}} \end{bmatrix}) = \text{softmax}(\begin{bmatrix} \hat{x}_i \mathbf{X}_D^\top & \hat{x}_i \hat{\mathbf{x}}^\top \end{bmatrix}) \begin{bmatrix} \mathbf{X}_D \\ \hat{\mathbf{x}} \end{bmatrix}, \quad (1)$$

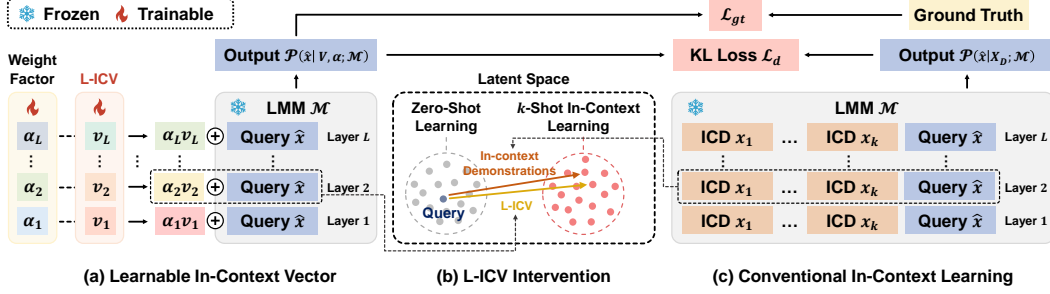


Figure 2: The L-ICV training pipeline: (a) The distribution $\mathcal{P}(\hat{x}|\mathbf{V}, \alpha; \mathcal{M})$ of LMMs output when using L-ICV. (b) Adding L-ICV into the representations of the query to simulate the shift effect brought by demonstrations. (c) The distribution $\mathcal{P}(\hat{x}|\mathbf{X}_D; \mathcal{M})$ of LMMs output when using demonstrations.

where vector $[\hat{x}_i \mathbf{X}_D^\top \quad \hat{x}_i \hat{x}^\top] \in \mathbb{R}^{1 \times l}$ and l denotes the sequence length of the entire input $[\mathbf{X}_D, \hat{x}]$. Expanding the softmax function, we obtain:

$$\begin{aligned} \text{softmax}([\hat{x}_i \mathbf{X}_D^\top \quad \hat{x}_i \hat{x}^\top]) &= \left[\underbrace{\frac{\exp(\hat{x}_i \mathbf{X}_D^\top)_1}{Z_1 + Z_2}, \dots, \frac{\exp(\hat{x}_i \mathbf{X}_D^\top)_{l_c}}{Z_1 + Z_2}}_{\text{expansion of } \hat{x}_i \mathbf{X}_D^\top}, \underbrace{\frac{\exp(\hat{x}_i \hat{x}^\top)_1}{Z_1 + Z_2}, \dots, \frac{\exp(\hat{x}_i \hat{x}^\top)_{l_q}}{Z_1 + Z_2}}_{\text{expansion of } \hat{x}_i \hat{x}^\top} \right] \\ &= \left[\frac{\exp(\hat{x}_i \mathbf{X}_D^\top)}{Z_1 + Z_2} \quad \frac{\exp(\hat{x}_i \hat{x}^\top)}{Z_1 + Z_2} \right], \end{aligned} \quad (2)$$

where l_c and l_q represent the lengths of the \mathbf{X}_D and \hat{x} , respectively. Z_1 and Z_2 are the sum of exponential scores between the query token \hat{x}_i with each token in \mathbf{X}_D and \hat{x} : $Z_1 = \sum_{l_c} \exp(\hat{x}_i \mathbf{X}_D^\top)$ and $Z_2 = \sum_{l_q} \exp(\hat{x}_i \hat{x}^\top)$. This leads to the following formulation of SA:

$$\begin{aligned} \text{SA}(\hat{x}_i, \mathbf{X}, \mathbf{X}) &= \frac{\exp(\hat{x}_i \mathbf{X}_D^\top) \mathbf{X}_D}{Z_1 + Z_2} + \frac{\exp(\hat{x}_i \hat{x}^\top) \hat{x}}{Z_1 + Z_2} \\ &= \frac{Z_1}{Z_1 + Z_2} \frac{\exp(\hat{x}_i \mathbf{X}_D^\top) \mathbf{X}_D}{Z_1} + \frac{Z_2}{Z_1 + Z_2} \frac{\exp(\hat{x}_i \hat{x}^\top)}{Z_2} \\ &= \frac{Z_1}{Z_1 + Z_2} \text{softmax}(\hat{x}_i \mathbf{X}_D^\top) \mathbf{X}_D + \frac{Z_2}{Z_1 + Z_2} \text{softmax}(\hat{x}_i \hat{x}^\top) \hat{x} \\ &= \mu \text{SA}(\hat{x}_i, \mathbf{X}_D, \mathbf{X}_D) + (1 - \mu) \text{SA}(\hat{x}_i, \hat{x}, \hat{x}), \end{aligned} \quad (3)$$

where $\mu = Z_1 / (Z_1 + Z_2)$. Let $h(z) = \text{SA}(\hat{x}_i, z, z)$. The output of $\text{SA}(\hat{x}_i)$ can then be expressed as:

$$\text{SA}(\hat{x}_i, \mathbf{X}, \mathbf{X}) = \mu h(\mathbf{X}_D) + (1 - \mu) h(\hat{x}) \quad (4)$$

As noted in Equation 4, we observe that $h(\hat{x})$ is the representation obtained with self-attention over the query \hat{x} without appending any ICD; $h(\mathbf{X}_D)$ functions similarly to a ‘‘shift’’ vector, altering the attention representation $h(\hat{x})$ by incorporating contextual information from the ICDs \mathbf{X}_D . The coefficient μ quantifies the degree of influence \mathbf{X}_D has over the original query representation. For a visual demonstration of how ICDs shift the representation space, see Figure 2 (b). Consequently, once learning a general shift direction to replace the effect of $h(\mathbf{X}_D)$, we can employ this shift direction to simulate the ICL process of LMMs without actual demonstrations.

We propose a novel method that involves a **Learnable In-Context Vector** (L-ICV) to simulate the ICL process without actual demonstrations. This approach aims to abstract general task information from demonstrations, enabling it to shift the model’s representation toward the direction influenced by the ICDs. Figure 2 shows the training pipeline of L-ICV. The L-ICV training dataset, denoted as $\mathcal{D} = \{d_1, \dots, d_N\}$, is a subset of the VQA dataset training split, created by randomly selecting N question-answer pairs from it. We use each training sample d_i to simulate the query sample \hat{x} in ICL, and randomly select k demonstrations from $\mathcal{D} \setminus \{d_i\}$ for it. Additionally, [22] shows that during ICL, each layer of an LLM performs a distinct role. Motivated by this, we assume that for LMM, each layer also requires a specific shift direction. We assign a learnable vector v_l and a weight factor

α_l for each layer l to learn the unique shift effect. Our final L-ICV comprises of the vector set \mathbf{V} and the corresponding weight factor set α as:

$$\begin{aligned}\mathbf{V} &= \{\mathbf{v}_1, \mathbf{v}_2, \dots, \mathbf{v}_L\}, \quad \mathbf{v}_i \in \mathbb{R}^{1 \times d} \\ \alpha &= \{\alpha_1, \alpha_2, \dots, \alpha_L\}, \quad \alpha_i \in \mathbb{R}^{1 \times 1},\end{aligned}\tag{5}$$

where L is the number of layers. To train \mathbf{V} and α , we align the distribution of the model’s outputs for the query when shifted by demonstrations, $\mathcal{P}(\hat{\mathbf{x}}|\mathbf{X}_D; \mathcal{M})$, with that shifted by our L-ICV, $\mathcal{P}(\hat{\mathbf{x}}|\mathbf{V}, \alpha; \mathcal{M})$. This alignment is achieved by minimizing the Kullback-Leibler (KL) divergence:

$$\mathcal{L}_d = \text{KL}(\mathcal{P}(\hat{\mathbf{x}}|\mathbf{X}_D; \mathcal{M}) \parallel \mathcal{P}(\hat{\mathbf{x}}|\mathbf{V}, \alpha; \mathcal{M}))\tag{6}$$

To obtain the distribution $\mathcal{P}(\hat{\mathbf{x}}|\mathbf{X}_D; \mathcal{M})$, for each query $\hat{\mathbf{x}}$, we randomly select k demonstrations to form \mathbf{X}_D . These are concatenated with the query to form the inputs for the model. The model’s output for the query is then considered as the shifted distribution $\mathcal{P}(\hat{\mathbf{x}}|\mathbf{X}_D; \mathcal{M})$.

To obtain the output of $\hat{\mathbf{x}}$ by using L-ICV, at the l -th layer, we use the vector \mathbf{v}_l to shift original representation and get: $h(\hat{\mathbf{x}}_i)' = h(\hat{\mathbf{x}}_i) + \alpha_l \mathbf{v}_l$, which is shown in Figure 2(a). After applying L-ICV to shift the representations at each layer, we obtain the output distribution $\mathcal{P}(\hat{\mathbf{x}}|\mathbf{V}, \alpha; \mathcal{M})$. Notably, during training, \mathbf{X}_D for each query $\hat{\mathbf{x}}$ includes randomly sampled 32-shot demonstrations. This strategy encourages our L-ICV to extract the most useful common information from various demonstration combinations and prevents it from being influenced by the individual characteristics of certain demonstrations.

In addition, to facilitate the L-ICV in acquiring more task-specific information, we also optimize the $\mathcal{P}(\hat{\mathbf{x}}|\mathbf{V}, \alpha; \mathcal{M})$ with the ground truth by \mathcal{L}_{gt} . Thus, the overall loss \mathcal{L} is defined as:

$$\begin{aligned}\mathcal{L} &= \lambda \mathcal{L}_{\text{gt}} + \mathcal{L}_d, \\ \text{where } \mathcal{L}_{\text{gt}} &= - \sum_i \log \mathcal{P}(\hat{\mathbf{x}}_i | \mathbf{V}, \alpha; \mathcal{M}).\end{aligned}\tag{7}$$

where λ is the hyper-parameter to control the importance of ground truth loss.

4 Experiments

4.1 Setting and implementation details

Model and Dataset: We evaluate our approach using the IDEFICS-9B model [7] across two datasets: VQAv2 [37] and OKVQA [38]. **VQAv2** emphasizes open-ended VQA tasks, encompassing 4, 437, 570 question-answer pairs in its training split, supplemented by an additional 2, 143, 540 pairs in the validation split. **OKVQA** is a large-scale dataset designed for models that require external knowledge to answer questions. It consists of 14, 055 question-answer pairs, with 9, 009 allocated for training and 5, 046 for validation. For both VQAv2 and OKVQA datasets, We train our L-ICV on 8, 000 pairs from each training set. Due to computational resource limitations, we randomly sample 10, 000 question-answer pairs from the VQAv2 validation split for evaluation [16]. For OKVQA, we utilize the entire validation split.

L-ICV Setting: During training, we assign 32-shot demonstrations for each query, enabling L-ICV to acquire better directions of shifting vectors for VQA tasks. The \mathbf{v}_i is initialized using a normal distribution with a mean of 0 and a standard deviation of 0.01, and all α_i are initialized to 0.1. More detailed training parameters can be found in Appendix.

4.2 Results

4.2.1 Compared Methods

We primarily compare the following methods:

Zero-Shot: The model uses only the query as input.

k-Shot ICL:The model uses k demonstrations, randomly selected from the VQA dataset training split, along with the query as input.

Non-Learnable ICV Methods: We extend three established non-learnable ICV methods from language models to our multimodal settings: (1) **Task Vector (TV)** [18] uses k demonstrations and a dummy query to extract the representation of the last token from a middle layer of the model

Table 1: Accuracy (%) with Different ICVs Methods and Finetuning Methods, where numbers in parentheses indicate multiples of L-ICV trainable parameters.

	Zero-Shot	32-shot ICL	TV	FV	PCA-ICV	LoRA	L-ICV (Ours)
VQAv2	29.25	56.18	43.68	30.21	34.75	49.02	58.54
OKVQA	30.54	48.48	32.68	31.02	30.59	34.21	50.08
Total Trainable Parameters	-	-	-	-	-	1, 155, 136($\times 8.8$)	131, 104($\times 1.0$)

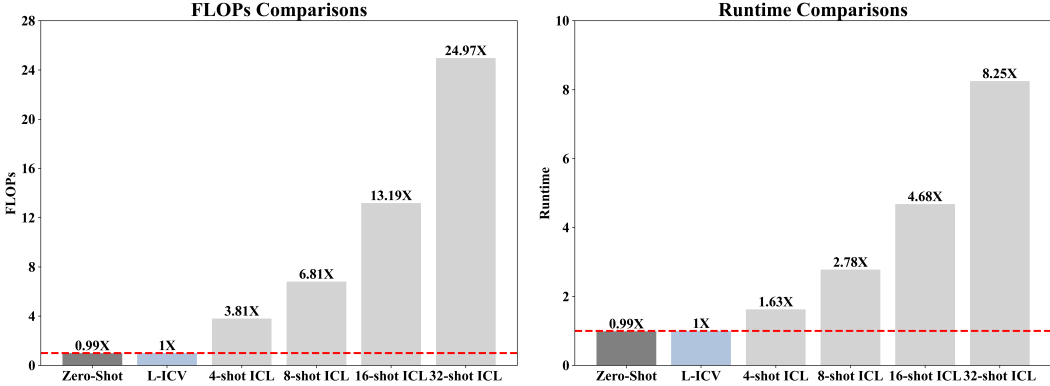


Figure 3: The total number of FLOPs and real inference time consumption of ICL, Zero-Shot, L-ICV for 1000 query samples.

as the ICV. During inference, this vector replaces the representation of the last token in the same layer. We conduct evaluations on **TV** by implementing it across various layers and select the layer where it achieves the highest performance improvement. (2) **Function Vector (FV)** [19] employs a small subset of the validation data to derive the mean output from critical attention heads, forming the ICV. During inference, this vector is added to the representations of the last token within a specific layer. We conduct evaluations on **FV** by implementing it across various layers and select the layer where it achieves the highest performance improvement. (3) **PCA In-Context Vector (PCA-ICV)** [20] computes the ICV by applying PCA to the difference between the question and question-answer representations from k demonstrations. During inference, these vectors are added to the representations of all tokens at each layer,

LoRA [23]: This method finetunes the LMMs with the same number of samples of training L-ICV. We add the LoRA module in the token classification head of the last layer. In this way, the number of trainable parameters is comparable to that of L-ICV.

4.2.2 Performance and Inference Efficiency on VQA.

We present performance comparisons with various methods in Table 1. Certain existing methods show only marginal improvements over Zero-Shot baselines, *e.g.*, FV improves by 0.96/0.48 on VQAv2/OKVQA and PCA-ICV improves by 0.04 on OKVQA. Besides, we observe that all the previous non-learnable ICV methods do not reach the performance of the standard 32-shot ICL, *e.g.*, the best non-learnable method, TV, is still 12.5/15.8 lower than 32-shot ICL on VQAv2/OKVQA. In contrast, our L-ICV achieves an accuracy improvement of 2.36 on VQAv2 and 1.6 on OKVQA over 32-shot ICL. These results highlight the inefficacy of non-learnable methods in capturing essential task-specific information for VQA, whereas L-ICV, by leveraging diverse 32-shot ICL demonstrations for each query during training, manages to abstract useful task information effectively. We further show that our L-ICV outperforms LoRA with less trainable parameters, suggesting L-ICV can abstract task information more efficiently.

Figure 3 displays the efficiency of L-ICV during inference compared to other methods. We average the FLOPs and actual inference time consumption per forward pass over 1000 randomly sampled queries.¹ We observe that L-ICV only needs 1/24.97 FLOPs and 1/8.25 inference time of 32-shot ICL per forward pass. Additionally, L-ICV maintains almost the same inference speed as Zero-Shot. These comparisons validate the efficiency of L-ICV during inference.

¹For detailed hardware information, refer to Appendix.

4.3 Ablation Studies

We use ablation studies to explore the effects of diverse settings, including different training losses, the shot number of demonstrations k used during training, and the number of training data N .

Training Loss: Table 2 compares the results of using different losses: only \mathcal{L}_{gt} in Eq. (7) or \mathcal{L}_d in Eq. (7). We find that only using \mathcal{L}_{gt} (same as standard fine-tuning) significantly damages the performance, *e.g.*, \mathcal{L}_{gt} achieves 16.9/6.12 lower accuracy on VQAv2/OKVQA compared to using the combined loss \mathcal{L} ; yet using only \mathcal{L}_d results in a smaller performance drop – 3.78/3.14 lower VQAv2/OKVQA than when using \mathcal{L} . This suggests that with a limited number of trainable parameters, L-ICV trained with \mathcal{L}_d is more robust and capable of capturing essential task information than \mathcal{L}_{gt} . It underscores that the L-ICV cannot solely rely on fine-tuning with LMMs on specific datasets, but should effectively leverage abstracted insights from demonstrations.

Table 2: Accuracy (%) of L-ICV with Different Training Loss on VQA.

	\mathcal{L}_d	\mathcal{L}_{gt}	\mathcal{L}
VQAv2	54.76	41.64	58.54
OKVQA	46.94	43.96	50.08

Number of Demonstrations k : We compare the performance of L-ICV trained with k demonstrations per query and the corresponding k -shot ICL in Table 3. The result shows that an increase in the number of demonstrations enhances the performance of ICL and L-ICV, indicating that more demonstrations can provide each query with a richer context to help train L-ICV. Additionally, L-ICV consistently surpasses the performance of k -shot ICL across different training sizes, showcasing the robustness of our L-ICV in utilizing demonstrations. Notably, when the number of demonstrations is limited, the performance gap between L-ICV and ICL becomes more pronounced. This is because ICL is highly sensitive to the choice of demonstrations; with insufficient demonstrations, the model may shift the query representations in an incorrect direction. In contrast, L-ICV continuously by learning the main shift direction of the query representations from the demonstrations, reduces the negative impact of poor demonstrations on the query during training and is more robust that can extract essential task information.

Table 3: Accuracy (%) of Different Number of Demonstrations on VQA.

Task	Method	Number of Demonstrations				
		1	4	8	16	32
VQAv2	L-ICV	56.84	57.60	58.25	58.27	58.54
	ICL	51.39	53.72	54.24	55.70	56.18
OKVQA	L-ICV	47.51	47.68	49.40	49.71	50.08
	ICL	40.75	46.11	46.79	47.70	48.48

Size of Training Set: Figure 4 illustrates how varying the number of training samples impacts the performance of L-ICV and LoRA. On the VQAv2 dataset, both methods show improved performance with increasing data sizes. Notably, L-ICV performs exceptionally well across both low and high training sizes. It achieves performance close to that of 1-shot ICL with just 700 training samples and surpasses 32-shot ICL with 4,000 training samples. In contrast, LoRA does not exceed the performance of 1-shot ICL, even when expanded to 8,000 samples. For OKVQA, the performance of LoRA with small data sizes is even worse than Zero-Shot. This is because OKVQA requires external knowledge to answer questions, while learning external knowledge from a small amount of data can disrupt the inherent knowledge of the pre-trained model, leading to a significant drop in performance. Conversely, L-ICV excels by focusing on learning shift direction, thus preserving the model’s inherent reasoning abilities. With just 500 samples, L-ICV outperforms 1-shot ICL, and with 4,000 samples, it nearly matches the performance of 32-shot ICL. These observations underscore L-ICV’s superior efficiency over LoRA in capturing and utilizing complex reasoning capabilities with much fewer training samples.

4.4 Analysis

4.4.1 The Shifting Effect in Latent Space

To better demonstrate the shifting effect of L-ICV on query samples, we randomly select 200 query samples and conduct different methods of inference in LMMs. We extract the representation vector of the first answer token for T-SNE dimensionality reduction, shown in Figure 5. Additionally, to quantitatively evaluate the effect of shift directions of different ICV methods, we calculate the following metrics. Given a query \hat{x} , we use r_{icl} , r_{zs} , r^* to denote the representation of the first answer token obtained by 32-shot ICL, Zero-Shot, specific ICV meth-

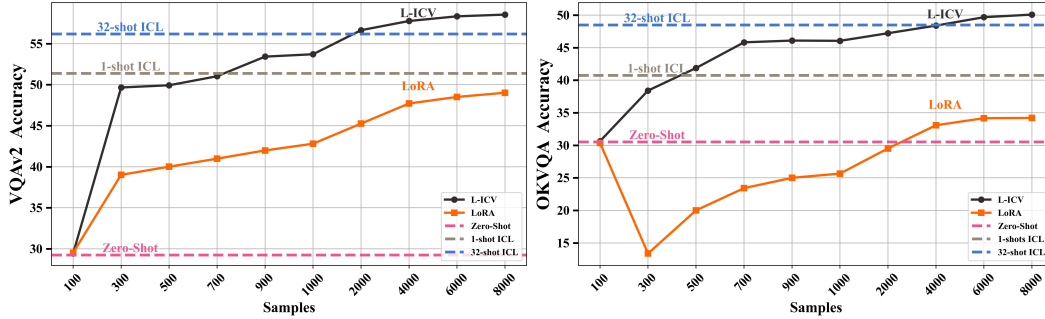


Figure 4: Accuracy (%) of L-ICV and LoRA with different size of training set.

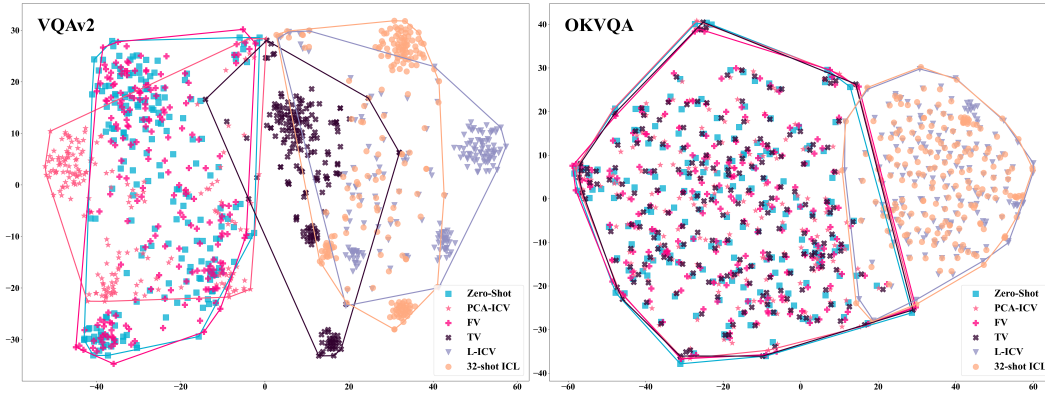


Figure 5: T-SNE visualization of first answer token representations over 200 queries.

Table 5: Direct decoding of the different ICV methods.

Methods	Decoding Top-10 Tokens of different methods in order of decreasing probability
TV	'No', 'Yes', 'no', 'It', 'I', 'No', 'The', 'A', 'yes', 'Not'
FV	':', 'in', ',', '(', 'for', 'and', '...', 'to', 'on', 'I'
PCA-ICV	'none', 'there', 'no', 'the', 'not', 'None', 'dep', '_yes', 'unknown', 'yes'
L-ICV	'Question', '_Short', '??', 'no', 'QUEST', 'questions', '\$?', 'answer', 'Short', '_questions'

ods, respectively. Then we calculate the standard shift direction as $s_{gt} = r_{icl} - r_{zs}$ and the shift direction of specific ICV as $s^* = r^* - r_{zs}$. Finally, we define the shift direction similarity as the cosine similarity between s^* and s_{gt} , indicating how closely the shift direction of the ICV method aligns with the standard shift direction. The results are presented in Table 4. From Figure 5, we can find that 32-shot ICL exhibits a significant shift compared to Zero-Shot, visualizing the shift effects given in Eq. 4. Considering both Table 4 and 1, we find that the shift direction similarity has positive correlation to the accuracy: if a method has large direction similarity, it also has better performance. For example, among non-learnable methods, TV has higher shift direction similarity than other ones, then it has better accuracy in Table 1. Furthermore, for L-ICV which has the best accuracy in Table 1, its shift direction similarity is also the highest, which is 0.742/0.829 on VQAv2/OKVQA, validating that L-ICV can produce shifts in query samples similar to 32-shot ICL, as visualized in Figure 5. Such positive correlation validates the effectiveness of our motivation that a single L-ICV can indeed simulate the ICL capability of LMMs by shifting the direction of the query representation.

4.4.2 Why Non-Learnable Methods are Poor on VQA?

Decoding ICV To Tokens: We follow previous studies [39–41] to analyze the parameters of

Table 4: The shift direction similarities of different ICV methods.

	TV	FV	PCA-ICV	L-ICV
VQAv2	0.486	-0.106	0.027	0.742
OKVQA	0.326	0.218	-0.190	0.829

Table 6: The frequency of yes/no hallucinations and meaningless responses.

	Zero-Shot	TV	FV	PCA-ICV	L-ICV
yes/no Hallucination	5	111	7	4	3
Meaningless Answer in yes/no	0	0	0	2	0
Meaningless Answer in number	2	0	2	522	0
Meaningless Answer in other	257	0	247	2072	2

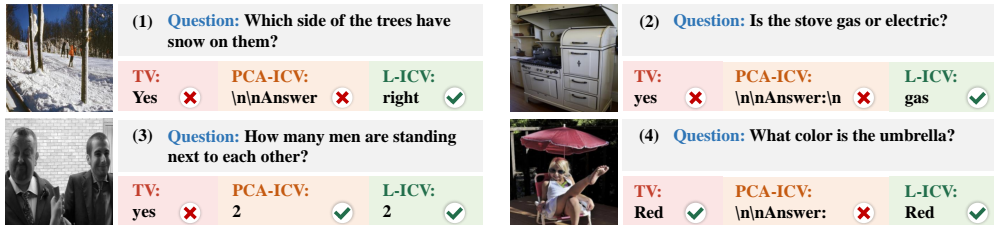


Figure 6: Visualizations of the cases where non-learnable methods appear yes/no hallucinations and meaningless responses.

Transformers by directly decoding them into vocabulary tokens. Specifically, given a vector $v \in \mathbb{R}^{1 \times d}$, it can be projected using the unembedding matrix $\mathbf{E} \in \mathbb{R}^{d \times \mathcal{N}}$ of LMMs to obtain the corresponding token probability distribution p , where \mathcal{N} is the vocabulary size:

$$p = \text{softmax}(v \cdot \mathbf{E}) = \frac{\exp(v \cdot \mathbf{E})}{\sum_j \exp(v \cdot \mathbf{E})_j}. \quad (8)$$

We calculate the p of the vectors got from different methods in VQAv2 and select the top-10 tokens with the highest probabilities in p shown in Table 5. We can see that the tokens got from FV are not highly relevant to the VQA task, which proves that FV does not capture the task information of VQAv2. On the other hand, the frequency of "yes" and "no" tokens is relatively high in the decoding results of PCA-ICV and TV, suggesting that they prefer to capture the simple patterns from demonstrations, *e.g.* yes/no, but struggle to grasp the overall task information of complex VQA. In contrast, the tokens of L-ICV decoding are not biased to specific answers like yes/no, suggesting it abstracts more summary task knowledge of VQA.

Hallucinations and Invalid Responses.

VQA contains various answer types and for convenience, VQAv2 divides them into three categories: "yes/no", "number", and "other". After delving deeper into the answer details, interestingly, we find that TV frequently answers "yes or no" to number/other questions as shown in Figure 6 (1)(2)(3). We term this phenomenon the **yes/no hallucination** and count the frequency of the yes/no hallucination over all test data samples for different methods in Table 6. We can find that TV appears 111 times of yes/no hallucination, being consistent with the observations in Table 5, suggesting TV is biased to yes/no type question. We also observe that non-learnable methods tend to respond meaningless text (*e.g.* "\n") when responding to "number/other" questions as shown in Figure 6 (1)(2)(4). Table 6 shows the number of meaningless answers. We find that PCA-ICV and TV have more chance to return meaningless answers for "other" questions, suggesting these methods do not capture the overall task information of VQA and are not able to answer some less frequently appeared questions. However, for L-ICV, it has less yes/no hallucination and meaningless responses, validating that L-ICV captures more robust task information of VQA.

5 Conclusion

To address the two major drawbacks of ICL in LMM—long computation time and sensitivity to demonstration selection—we try to apply non-learnable ICV methods from NLP to solve VQA. However, due to the complexity of VQA and the significant biases often inherent in non-learnable methods, the performance is unsatisfactory. Then we propose the Learnable ICV (L-ICV) to overcome this drawback. By learning the general shift direction from a large amount of ICL data, L-ICV successfully replaces the role of demonstrations in ICL. Experiments validate that L-ICV outperforms traditional ICL methods and other non-learnable ICV methods on two VQA datasets. Experiments also show that L-ICV, compared to LoRA, maintains excellent performance with minimal data,

suggesting L-ICV is a new research direction for LMMs to solve multimodal tasks. In the future, we will explore the application of L-ICV on more multimodal tasks by various LMMs.

References

- [1] Josh Achiam, Steven Adler, Sandhini Agarwal, Lama Ahmad, Ilge Akkaya, Florencia Leoni Aleman, Diogo Almeida, Janko Altenschmidt, Sam Altman, Shyamal Anadkat, et al. Gpt-4 technical report. *ArXiv preprint*, abs/2303.08774, 2023.
- [2] Hugo Touvron, Thibaut Lavril, Gautier Izacard, Xavier Martinet, Marie-Anne Lachaux, Timothée Lacroix, Baptiste Rozière, Naman Goyal, Eric Hambro, Faisal Azhar, et al. Llama: Open and efficient foundation language models. *ArXiv preprint*, abs/2302.13971, 2023.
- [3] Hugo Touvron, Louis Martin, Kevin Stone, Peter Albert, Amjad Almahairi, Yasmine Babaei, Nikolay Bashlykov, Soumya Batra, Prajjwal Bhargava, Shruti Bhosale, et al. Llama 2: Open foundation and fine-tuned chat models. *ArXiv preprint*, abs/2307.09288, 2023.
- [4] Jiachang Liu, Dinghan Shen, Yizhe Zhang, Bill Dolan, Lawrence Carin, and Weizhu Chen. What makes good in-context examples for GPT-3? In *Proceedings of Deep Learning Inside Out (DeeLIO 2022): The 3rd Workshop on Knowledge Extraction and Integration for Deep Learning Architectures*, pages 100–114, Dublin, Ireland and Online, 2022. Association for Computational Linguistics.
- [5] Qingxiu Dong, Lei Li, Damai Dai, Ce Zheng, Zhiyong Wu, Baobao Chang, Xu Sun, Jingjing Xu, and Zhifang Sui. A survey on in-context learning. *ArXiv preprint*, abs/2301.00234, 2023.
- [6] Jean-Baptiste Alayrac, Jeff Donahue, Pauline Luc, Antoine Miech, Iain Barr, Yana Hasson, Karel Lenc, Arthur Mensch, Katherine Millican, Malcolm Reynolds, et al. Flamingo: a visual language model for few-shot learning. *Advances in neural information processing systems*, 35:23716–23736, 2022.
- [7] Hugo Laurençon, Lucile Saulnier, Léo Tronchon, Stas Bekman, Amanpreet Singh, Anton Lozhkov, Thomas Wang, Siddharth Karamcheti, Alexander M. Rush, Douwe Kiela, Matthieu Cord, and Victor Sanh. Obelics: An open web-scale filtered dataset of interleaved image-text documents, 2023.
- [8] Maria Tsimpoukelli, Jacob Menick, Serkan Cabi, S. M. Ali Eslami, Oriol Vinyals, and Felix Hill. Multimodal few-shot learning with frozen language models. In Marc’Aurelio Ranzato, Alina Beygelzimer, Yann N. Dauphin, Percy Liang, and Jennifer Wortman Vaughan, editors, *Advances in Neural Information Processing Systems 34: Annual Conference on Neural Information Processing Systems 2021, NeurIPS 2021, December 6-14, 2021, virtual*, pages 200–212, 2021.
- [9] Feng Nie, Meixi Chen, Zhirui Zhang, and Xu Cheng. Improving few-shot performance of language models via nearest neighbor calibration. *ArXiv preprint*, abs/2212.02216, 2022.
- [10] Yao Lu, Max Bartolo, Alastair Moore, Sebastian Riedel, and Pontus Stenetorp. Fantastically ordered prompts and where to find them: Overcoming few-shot prompt order sensitivity. In *Proceedings of the 60th Annual Meeting of the Association for Computational Linguistics (Volume 1: Long Papers)*, pages 8086–8098, Dublin, Ireland, 2022. Association for Computational Linguistics.
- [11] Tianyu Gao, Adam Fisch, and Danqi Chen. Making pre-trained language models better few-shot learners. In *Proceedings of the 59th Annual Meeting of the Association for Computational Linguistics and the 11th International Joint Conference on Natural Language Processing (Volume 1: Long Papers)*, pages 3816–3830, Online, 2021. Association for Computational Linguistics.
- [12] Zhiyong Wu, Yaoxiang Wang, Jiacheng Ye, and Lingpeng Kong. Self-adaptive in-context learning: An information compression perspective for in-context example selection and ordering. *ArXiv preprint*, abs/2212.10375, 2022.
- [13] Tai Nguyen and Eric Wong. In-context example selection with influences. *ArXiv preprint*, abs/2302.11042, 2023.
- [14] Xiaonan Li and Xipeng Qiu. Finding supporting examples for in-context learning. *arXiv e-prints*, pages arXiv–2302, 2023.

- [15] Yiming Zhang, Shi Feng, and Chenhao Tan. Active example selection for in-context learning. In *Proceedings of the 2022 Conference on Empirical Methods in Natural Language Processing*, pages 9134–9148, Abu Dhabi, United Arab Emirates, 2022. Association for Computational Linguistics.
- [16] Li Li, Jiawei Peng, Huiyi Chen, Chongyang Gao, and Xu Yang. How to configure good in-context sequence for visual question answering. *ArXiv preprint*, abs/2312.01571, 2023.
- [17] Xu Yang, Yongliang Wu, Mingzhuo Yang, Haokun Chen, and Xin Geng. Exploring diverse in-context configurations for image captioning. *Advances in Neural Information Processing Systems*, 36, 2024.
- [18] Roeel Hendel, Mor Geva, and Amir Globerson. In-context learning creates task vectors. *ArXiv preprint*, abs/2310.15916, 2023.
- [19] Eric Todd, Millicent L Li, Arnab Sen Sharma, Aaron Mueller, Byron C Wallace, and David Bau. Function vectors in large language models. *ArXiv preprint*, abs/2310.15213, 2023.
- [20] Sheng Liu, Lei Xing, and James Zou. In-context vectors: Making in context learning more effective and controllable through latent space steering. *ArXiv preprint*, abs/2311.06668, 2023.
- [21] Kim Anh Nguyen, Sabine Schulte im Walde, and Ngoc Thang Vu. Distinguishing antonyms and synonyms in a pattern-based neural network. In *Proceedings of the 15th Conference of the European Chapter of the Association for Computational Linguistics: Volume 1, Long Papers*, pages 76–85, Valencia, Spain, 2017. Association for Computational Linguistics.
- [22] Lean Wang, Lei Li, Damai Dai, Deli Chen, Hao Zhou, Fandong Meng, Jie Zhou, and Xu Sun. Label words are anchors: An information flow perspective for understanding in-context learning. *ArXiv preprint*, abs/2305.14160, 2023.
- [23] Edward J. Hu, Yelong Shen, Phillip Wallis, Zeyuan Allen-Zhu, Yuanzhi Li, Shean Wang, Lu Wang, and Weizhu Chen. Lora: Low-rank adaptation of large language models. In *The Tenth International Conference on Learning Representations, ICLR 2022, Virtual Event, April 25-29, 2022*. OpenReview.net, 2022.
- [24] Tom B. Brown, Benjamin Mann, Nick Ryder, Melanie Subbiah, Jared Kaplan, Prafulla Dhariwal, Arvind Neelakantan, Pranav Shyam, Girish Sastry, Amanda Askell, Sandhini Agarwal, Ariel Herbert-Voss, Gretchen Krueger, Tom Henighan, Rewon Child, Aditya Ramesh, Daniel M. Ziegler, Jeffrey Wu, Clemens Winter, Christopher Hesse, Mark Chen, Eric Sigler, Mateusz Litwin, Scott Gray, Benjamin Chess, Jack Clark, Christopher Berner, Sam McCandlish, Alec Radford, Ilya Sutskever, and Dario Amodei. Language models are few-shot learners. In Hugo Larochelle, Marc’Aurelio Ranzato, Raia Hadsell, Maria-Florina Balcan, and Hsuan-Tien Lin, editors, *Advances in Neural Information Processing Systems 33: Annual Conference on Neural Information Processing Systems 2020, NeurIPS 2020, December 6-12, 2020, virtual*, 2020.
- [25] Alec Radford, Jeffrey Wu, Rewon Child, David Luan, Dario Amodei, Ilya Sutskever, et al. Language models are unsupervised multitask learners. *OpenAI blog*, 1(8):9, 2019.
- [26] Yu Sun, Shuohuan Wang, Shikun Feng, Siyu Ding, Chao Pang, Junyuan Shang, Jiayang Liu, Xuyi Chen, Yanbin Zhao, Yuxiang Lu, et al. Ernie 3.0: Large-scale knowledge enhanced pre-training for language understanding and generation. *ArXiv preprint*, abs/2107.02137, 2021.
- [27] Marius Mosbach, Tiago Pimentel, Shauli Ravfogel, Dietrich Klakow, and Yanai Elazar. Few-shot fine-tuning vs. in-context learning: A fair comparison and evaluation. In Anna Rogers, Jordan Boyd-Graber, and Naoaki Okazaki, editors, *Findings of the Association for Computational Linguistics: ACL 2023*, pages 12284–12314, Toronto, Canada, July 2023. Association for Computational Linguistics.
- [28] Yaru Hao, Yutao Sun, Li Dong, Zhixiong Han, Yuxian Gu, and Furu Wei. Structured prompting: Scaling in-context learning to 1,000 examples. *arXiv preprint arXiv:2212.06713*, 2022.
- [29] Xinyi Wang, Wanrong Zhu, Michael Saxon, Mark Steyvers, and William Yang Wang. Large language models are latent variable models: Explaining and finding good demonstrations for in-context learning. *Advances in Neural Information Processing Systems*, 36, 2024.

- [30] Guangxuan Xiao, Yuandong Tian, Beidi Chen, Song Han, and Mike Lewis. Efficient streaming language models with attention sinks. *arXiv preprint arXiv:2309.17453*, 2023.
- [31] Hanshi Sun, Zhuoming Chen, Xinyu Yang, Yuandong Tian, and Beidi Chen. Triforce: Lossless acceleration of long sequence generation with hierarchical speculative decoding. *arXiv preprint arXiv:2404.11912*, 2024.
- [32] Yichen Zhu, Minjie Zhu, Ning Liu, Zhicai Ou, Xiaofeng Mou, and Jian Tang. Llava- ϕ : Efficient multi-modal assistant with small language model. *ArXiv preprint*, abs/2401.02330, 2024.
- [33] Haotian Liu, Chunyuan Li, Yuheng Li, and Yong Jae Lee. Improved baselines with visual instruction tuning. *ArXiv preprint*, abs/2310.03744, 2023.
- [34] Anas Awadalla, Irena Gao, Josh Gardner, Jack Hessel, Yusuf Hanafy, Wanrong Zhu, Kalyani Marathe, Yonatan Bitton, Samir Gadre, Shiori Sagawa, et al. Openflamingo: An open-source framework for training large autoregressive vision-language models. *ArXiv preprint*, abs/2308.01390, 2023.
- [35] Deyao Zhu, Jun Chen, Xiaoqian Shen, Xiang Li, and Mohamed Elhoseiny. Minigpt-4: Enhancing vision-language understanding with advanced large language models. *ArXiv preprint*, abs/2304.10592, 2023.
- [36] Bo Li, Yuanhan Zhang, Liangyu Chen, Jinghao Wang, Fanyi Pu, Jingkang Yang, Chunyuan Li, and Ziwei Liu. Mimic-it: Multi-modal in-context instruction tuning. *ArXiv preprint*, abs/2306.05425, 2023.
- [37] Yash Goyal, Tejas Khot, Douglas Summers-Stay, Dhruv Batra, and Devi Parikh. Making the V in VQA matter: Elevating the role of image understanding in visual question answering. In *2017 IEEE Conference on Computer Vision and Pattern Recognition, CVPR 2017, Honolulu, HI, USA, July 21-26, 2017*, pages 6325–6334. IEEE Computer Society, 2017.
- [38] Kenneth Marino, Mohammad Rastegari, Ali Farhadi, and Roozbeh Mottaghi. OK-VQA: A visual question answering benchmark requiring external knowledge. In *IEEE Conference on Computer Vision and Pattern Recognition, CVPR 2019, Long Beach, CA, USA, June 16-20, 2019*, pages 3195–3204. Computer Vision Foundation / IEEE, 2019.
- [39] Mor Geva, Roei Schuster, Jonathan Berant, and Omer Levy. Transformer feed-forward layers are key-value memories. *arXiv preprint arXiv:2012.14913*, 2020.
- [40] Nora Belrose, Zach Furman, Logan Smith, Danny Halawi, Igor Ostrovsky, Lev McKinney, Stella Biderman, and Jacob Steinhardt. Eliciting latent predictions from transformers with the tuned lens. *arXiv preprint arXiv:2303.08112*, 2023.
- [41] Guy Dar, Mor Geva, Ankit Gupta, and Jonathan Berant. Analyzing transformers in embedding space. *arXiv preprint arXiv:2209.02535*, 2022.
- [42] Diederik P. Kingma and Jimmy Ba. Adam: A method for stochastic optimization. In Yoshua Bengio and Yann LeCun, editors, *3rd International Conference on Learning Representations, ICLR 2015, San Diego, CA, USA, May 7-9, 2015, Conference Track Proceedings*, 2015.
- [43] Nitish Srivastava, Geoffrey Hinton, Alex Krizhevsky, Ilya Sutskever, and Ruslan Salakhutdinov. Dropout: a simple way to prevent neural networks from overfitting. *The journal of machine learning research*, 15(1):1929–1958, 2014.

A Implementation Details.

A.1 L-ICV Hyperparameters

Table 7 presents the hyper-parameters utilized for training the L-ICV. The optimizer denotes the optimization algorithm employed during model training. For V and α , we use different learning rate to optimize. The λ represents the weight assigned to \mathcal{L}_{gt} in Eq 7 during training. Precision refers to the float precision type used for model weights and gradient descent throughout the ICV training process. Weight Decay signifies the rate of weight decay applied during training, the warm up value is set to 0.01. while accumulate batches denotes the batch size for gradient accumulation during the training phase.

Table 7: VQAv2 and OKVQA L-ICV Training Parameters

Hyperparameter	VQAv2	OKVQA
optimizer	AdamW [42]	AdamW
learning rate of α	1e-2	1e-2
learning rate of V	1e-3	5e-3
λ	0.5	0.5
weight decay	1e-3	1e-3
precision	BF16	BF16
batch size	2	2
warm up	0.1	0.1
accumulate batches	8	8
number of epochs	10	10

A.2 LoRA Hyperparameters

Table 8 details the hyper-parameters for the LoRA model trained during our experiment. Both the OKVQA and VQAv2 datasets use the same hyper-parameters.

Table 8: LoRA Training Parameters

Hyperparameter	Value
optimizer	AdamW
learning rate	1e-3
LoRA matrix rank	32
LoRA dropout rate[43]	0.05
batch size	2
warm up	0.1
number of epochs	10

A.3 Inference and hardware details

In our ICV inference process, we employ the following hyperparameters: For ICV model inference, the maximum number of new tokens is set to 5, the number of beam searches is set to 3, the length penalty is set to 0, and the minimum number of generated tokens is set to 0. During the inference process, we utilize two Xeon Silver 3414 CPUs, one RTX 3090 GPU, and 384 GB of memory.

B Detailed Results

B.1 The Detailed Inference Speed Experiments

This subsection provides a detailed presentation of some experimental data, primarily including forward propagation FLOPs and runtime cost, as well as a comparison of specific data between L-ICV and LoRA. Table 9 presents the detailed results of the runtime and the FLOPs shown in Figure 3. For

a forward operation L-ICV compared to k-shot ICL. The average token length during the forward inference is 38 tokens for Zero-Shot and L-ICV, 107 tokens for 4-shot ICL, 187 tokens for 8-shot ICL, 330 tokens for 16-shot ICL, and 633 tokens for 32-shot ICL.

Table 9: Comparison of FLOPs and Runtime for L-ICV and k -shot ICL

Metric	Zero-Shot	L-ICV	4-shot ICL	8-shot ICL	16-shot ICL	32-shot ICL
FLOPs (TFLOPs)	0.935	0.936	3.568	6.375	12.341	23.364
Runtime (ms)	56.69	56.81	92.44	158.21	266.13	468.55

B.2 The Detailed Accuracy of Different Training Dataset

Table 10 presents a comparative analysis of the results between LoRA and L-ICV results on different training dataset size in Section 4.3.

B.3 Non-Learnable Methods Results

Function Vector: This section examines the test results of the function vector employed in the experiment across different layers of the IDEFICS-9B model. Table 11 presents the test results for VQAv2, and Table 12 shows the test results for OKVQA. The Best result of VQAv2 is 10th layer’s result, which reaches 30.21, and the best result of OKVQA is 31.02 from the first layer.

Table 10: Accuracy (%) of LoRA and L-ICV on different training set sizes

Dataset	Method	Training set size									
		100	300	500	700	900	1000	2000	4000	6000	8000
VQAv2	L-ICV	29.43	49.66	49.93	51.03	53.42	53.71	56.64	57.76	58.33	58.54
	LoRA	29.52	39.02	40.01	40.99	41.99	42.81	45.26	47.71	48.51	49.02
OKVQA	L-ICV	30.64	38.41	41.87	45.82	46.09	46.05	47.22	48.39	49.68	50.08
	LORA	30.37	13.38	20.01	23.42	25.01	25.66	29.52	33.08	34.17	34.21

Table 11: The Function Vector Accuracy (%) across different layers on VQAv2.

VQAv2	layer:1	layer:2	layer:3	layer:4	layer:5	layer:6	layer:7
	29.28	29.0	28.5	27.43	27.94	28.7	29.17
	layer:9	layer:10	layer:11	layer:12	layer:13	layer:14	layer:15
	29.34	30.21	29.94	29.48	29.52	29.38	29.62
	layer:17	layer:18	layer:19	layer:20	layer:21	layer:22	layer:23
	29.51	29.59	29.5	29.28	29.24	29.29	29.11
	layer:25	layer:26	layer:27	layer:28	layer:29	layer:30	layer:31
	29.34	29.19	29.26	29.18	29.19	29.45	29.32

Task Vector: This section examines the test results of the task vector utilized in the experiment across various layers of the IDEFICS model. Table 13 displays the test results for VQAv2, while Table 14 shows the test results for OKVQA. The task vector is derived using 32 question-answer pairs. The best result of the task vector on VQAv2 is at the 10th layer, reaching 43.68, while the best result on OKVQA is at the 12th layer, reaching 32.68.

PCA-ICV: PCA-ICV employs a weighting factor α to regulate the degree of interference ICV has on the model. We test various values of α to assess performance. Table 15 shows the results of PCA-ICV on VQAv2 and OKVQA datasets with different α value and extract samples. It is evident

Table 12: The Function Vector Accuracy (%) across different layers on OKVQA

OKVQA	layer:1	layer:2	layer:3	layer:4	layer:5	layer:6	layer:7	layer:8
	31.02	30.57	30.23	30.27	30.04	30.36	30.61	30.23
	layer:9	layer:10	layer:11	layer:12	layer:13	layer:14	layer:15	layer:16
	30.56	30.62	30.6	30.27	30.22	30.19	30.2	30.3
	layer:17	layer:18	layer:19	layer:20	layer:21	layer:22	layer:23	layer:24
	30.44	30.25	30.27	30.17	30.22	30.16	30.31	30.23
	layer:25	layer:26	layer:27	layer:28	layer:29	layer:30	layer:31	layer:32
	30.42	30.32	30.34	30.25	30.3	30.34	30.4	30.28

Table 13: The Task Vector Accuracy (%) across different layers on VQAv2

VQAv2	layer:1	layer:2	layer:3	layer:4	layer:5	layer:6	layer:7
	28.18	28.82	30.47	30.53	36.41	35.35	36.17
	layer:9	layer:10	layer:11	layer:12	layer:13	layer:14	layer:15
	41.72	43.68	40.33	34.32	16.91	15.42	14.53
	layer:17	layer:18	layer:19	layer:20	layer:21	layer:22	layer:23
	12.94	12.44	12.28	11.89	11.98	11.78	11.44
	layer:25	layer:26	layer:27	layer:28	layer:29	layer:30	layer:31
	12.8	12.95	12.97	12.86	12.87	13.29	14.7

Table 14: The Task Vector Accuracy (%) across different layers on OKVQA

OKVQA	layer:0	layer:1	layer:2	layer:3	layer:4	layer:5	layer:6	layer:7
	13.58	14.4	15.3	15.0	15.79	18.06	19.18	22.37
	layer:8	layer:9	layer:10	layer:11	layer:12	layer:13	layer:14	layer:15
	21.71	22.93	32.5	31.99	32.68	29.38	21.4	17.27
	layer:16	layer:17	layer:18	layer:19	layer:20	layer:21	layer:22	layer:23
	6.49	0.94	0.5	0.53	0.46	0.32	0.34	0.29
	layer:24	layer:25	layer:26	layer:27	layer:28	layer:29	layer:30	layer:31
	0.28	0.3	0.3	0.29	0.33	0.33	0.33	1.11

that the optimal alpha for the VQAv2 dataset significantly differs from that for OKVQA. The optimal result of PCA-ICV on VQAv2 is 34.75 when alpha is set to $1e-2$, while the best result for PCA-ICV is 30.59 when alpha is set to $1e-5$.

Table 15: The PCA-ICV Accuracy (%) across different alpha

Dataset	Samples	Alpha			
		$1e-2$	$1e-3$	$1e-4$	$1e-5$
VQAv2	32	34.75	30.95	30.06	30.0
OKVQA	32	22.46	30.06	30.23	30.59

C General L-ICV

L-ICV is essentially a shift vector, allowing us to control the shift directions of query representations, which means we can control the shift direction of LMMs by adding or subtracting different shift vectors. Therefore, we can use several L-ICV trained on different VQA dataset to get the **General L-ICV**. Specifically, given the diverse VQA task set $T = \{t_1, \dots, t_n\}$, where t_i is a VQA task and n is the number of tasks, we train the task-specific L-ICV $V^i = \{v_1^i, \dots, v_L^i\}$ and the weight factor $\alpha^i = \{\alpha_1^i, \dots, \alpha_L^i\}$ on each VQA dataset. Then, we have the L-ICV set $\mathcal{V}_{set} = \{V^1, \dots, V^n\}$ and its weight factors set $\alpha_{set} = \{\alpha^1, \dots, \alpha^n\}$. The General L-ICV has the same shape of task-specific L-ICV. For the l -th layer, it is defined as $v_l = \sum_i \alpha_l^i v_l^i$. During inference, we use the vector v_l to shift the original representation, resulting in $h(\hat{x}_i)' = h(\hat{x}_i) + v_l$. We average the L-ICV trained in OKVQA and VQAv2 to get the general ICV and evaluate the performance of the general ICV $V_g = \{v_1, \dots, v_L\}$ on OKVQA and VQAv2, with the results presented on Table 16.

Table 16: Accuracy (%) for 32-shot ICL, task-specific L-ICV, General L-ICV.

Methods	32-shot ICL	L-ICV	General L-ICV
VQAv2	56.18	58.54	56.17
OKVQA	48.48	50.08	49.52

The results indicate that while the performance of the general ICV is somewhat reduced compared to task-specific L-ICV; it decreased by 2.37 on VQAv2 and by 0.56 on OKVQA. However, its performance is very close to that of 32-shot ICL. Most importantly, it offers significant advantages in real-world scenarios where the distribution of test data is unknown. This makes the general ICV more suitable for practical applications, providing a robust solution that can be effectively utilized across varying environments. Furthermore, the findings highlight the scalability of L-ICV: whenever a new VQA dataset is used to train L-ICV, we only need to simply recalculate the mean shift vectors of all previously trained task-specific L-ICVs and the new L-ICV to generate a new general ICV, thus creating a more general VQA L-ICV. This approach not only simplifies the adaptation process for diverse tasks but also ensures that the model maintains a high level of performance across different applications. The results, therefore, underscore the potential of general ICVs to enhance the flexibility and applicability of VQA systems in real-world settings.